Title: Bioengineering of the implantable vascularized endocrine constructs for insulin delivery suitable for clinical upscaling

Authors: Kevin Bellofatto[1,2†], Fanny Lebreton[1,2†], Masoud Hassany[1‡], Reine Hanna[1,2], Juliette Bignard[1,2], Antoine Marteyn[1,2], Laura Mar Fonseca[1,2], Francesco Campo[8], Cristina Olgasi[7], Lelia Wolf-van Bürck[10], Mohsen Honarpisheh[10], Begoña Martinez de Tejada[11], Antonia Follenzi[6], Antonio Citro[8], Lorenzo Piemonti[8], Olivier Thaunat[9], Jochen Seissler[10], Phillippe Compagnon[1,3], Marie Cohen[11], Ekaterine Berishvili[1,2,3,4,5*] and VANGUARD consortium[§]

Affiliations:

[1]Cell Isolation and Transplantation Centre, Department of Surgery, Geneva University Hospitals, Geneva, Switzerland

[2]Laboratory of Tissue Engineering and Organ Regeneration, Department of Surgery, University of Geneva, Geneva, Switzerland

[3]Division of Transplantation, Department of Surgery, University of Geneva Hospitals, Geneva, Switzerland

[4]Faculty Diabetes Center, University of Geneva School of Medicine, Geneva, Switzerland

[5]Institute of Medical and Public Health Research, Ilia State University, Tbilisi, Georgia

[6]Department of Health Sciences, University of Piemonte Orientale, Novara, Italy

[7]Department of Translational Medicine, University of Piemonte Orientale, Novara, Italy

[8]IRCCS Ospedale San Raffaele, Diabetes Research Institute, Milano, Italy

[9]Lyon Claude Bernard University, Dept. Transplantation, Nephrology and Clinical Immunology, Lyon, France

[10]Medizinische Klinik und Poliklinik IV, Diabetes Zentrum, Klinikum der Universität München, LMU Munich, Germany

[11]Department of Pediatrics, Gynecology and Obstetrics, Faculty of Medicine, Geneva, Switzerland

*Corresponding author. Email: Ekaterine.berishvili@unige.ch

†These authors contributed equally to this work

‡Present address: Department of Civil and Mechanical Engineering, Technical University of Denmark, 2800 Kgs. Lyngby, Denmark

One Sentence Summary: A clinically scalable, biological hydrogel based vascularized endocrine constructs show sustained diabetes reversal.

Abstract:

Beta cell replacement therapy for type 1 diabetes is hindered by poor graft survival and suboptimal function, largely due to inadequate vascularization and lack of supportive microenvironment. To address these challenges, we developed a clinically scalable, extracellular matrix (ECM)–mimetic hydrogel, termed Amniogel, derived from human amniotic membrane via streamlined, clinically compliant process. Co-encapsulation of pancreatic islets with blood outgrowth endothelial cells (BOECs) within Amniogel facilitated the formation of prevascularized endocrine constructs (VECs). These constructs demonstrated enhanced β-cell viability and function through ECM-bound pro-survival signals, rapid self-assembly of perfusable endothelial networks enabling efficient glucose sensing, and deposition of laminin-rich basement membranes enhancing β-cell coupling and insulin secretion kinetics. In preclinical diabetic mouse models, VECs rapidly integrated with the host vasculature and provided sustained glycemic control when implanted subcutaneously. This integrative approach, combining a scalable, cost-effective biological scaffold with autologous vascularization potential, represents a significant advancement toward durable and clinically translatable β-cell replacement therapies for T1DM.

66 **INTRODUCTION**

67 Type 1 diabetes mellitus (T1DM) results from autoimmune destruction of insulin-producing β-
68 cells, and while insulin therapy is the standard treatment, it does not prevent long-term
69 complications or ease the daily management burdens (*1*). Intrahepatic islet transplantation
70 temporarily restores insulin independence and improves glycemic control (*2*). However, its
71 widespread clinical implementation is hindered by donor islet scarcity and the risks associated
72 with lifelong immunosuppression (*3-6*). Moreover, instant blood-mediated inflammatory reaction
73 (IBMIR), oxidative stress, loss of extracellular matrix (ECM) signals and poor vascularization
74 significantly compromise islet engraftment and function in the liver (*7-10*). Extrahepatic
75 transplantation sites are being explored to overcome these issues (*11-19*). Amongst these, the
76 subcutaneous space is gaining interest due to its safety, large surface area, and accessibility for
77 implantation and monitoring. However, inadequate vascularization and hypoxia frequently lead to
78 islet graft failure (*20, 21*).

79 Tissue-engineering approaches aim to mitigate these issues using supportive scaffolds or
80 encapsulation devices. Diverse macrodevices made of synthetic polymers have been designed to
81 house islets or stem cell–derived islet-like clusters (*22*). Although some have advanced to first-in-
82 human trials, clinical success has been limited due to fibrosis, foreign body response, and
83 inadequate vascularization (*23-25*). Critically, macro-devices designed so far rely on inorganic or
84 synthetic polymers, which fail to deliver the native ECM cues and vascularization essential for β-
85 cell survival and function.

86 Islets are abundantly vascularized miniorgans surrounded by specialized extracellular matrix
87 essential for β-cell viability and proper function (*26*). The isolation process disrupts this
88 irreversibly disrupts this dynamic microenvironment, triggering β-cell apoptosis (*27*). Integrating

ECM components with endothelial cells has been shown to improve islet survival and function in preclinical models (*28-32*). Yet, the clinical translation of these strategies remains challenging. An ideal construct would combine a biocompatible biological ECM with a built-in, high-density, functional vascular network in direct contact with encapsulated islets, enabling prompt revascularization, efficient glucose sensing and insulin secretion, and be readily scalable for clinical translation.

Here, we report a clinically scalable strategy to engineer vascularized endocrine constructs for subcutaneous implantation. We first generated Amniogel, an ECM-mimetic hydrogel derived from the human amniotic membrane, suitable for low-cost, clinical-grade manufacturing. By co-encapsulating pancreatic islets and blood outgrowth endothelial cells (BOECs) within this biologic platform, we engineered prevascularized endocrine constructs that replicate key aspects of the native islet niche through three synergistic mechanisms: 1) preservation of β-cell viability and function via essential ECM-bound pro-survival signals, 2) self-assembly of perfusable endothelial networks directly interfacing with islets to enable rapid glucose sensing and 3) deposition of laminin-rich basement membrane components that enhance β-cell gap junction coupling and insulin secretion kinetics. Importantly, engineered constructs demonstrated rapid vascular integration and sustained glycemic control in diabetic mice in two clinically relevant extrahepatic sites—the epididymal fat pad (as an omental analog in rodents) (*33, 34*) and the subcutaneous space. This synergistic strategy, integrating a clinically scalable biomaterial with autologous vascularization potential, represents a promising advance toward clinically translatable, durable cell therapies for type 1 diabetes.

112 **RESULTS**

113 **Production and characterization of Amniogel**

114 To enable clinical translation of Amniogel, we developed a five-step, Good Manufacturing
115 Practice (GMP)-compliant production protocol (Fig. 1A). Human amniotic membrane (hAM) was
116 decellularized using xenogen-free 10X TrypLE™ Select, effectively reducing DNA content from
117 424.0 ± 58.15 ng/mg in native tissue to 38.03 ± 2.24 ng/mg, below the biocompatibility threshold
118 of <50 ng/mg (Fig 1B) (*35*). Biochemical profiling confirmed retention of collagen, although
119 glycosaminoglycan content was partially decreased from 8.83 ± 1.18 to 3.59 ± 1.16 µg/mg (Fig.
120 1C–D).

121 Mass spectrometry confirmed retention of key ECM proteins known to support islets (*36*),
122 including collagen alpha-1(I) chain, collagen alpha-1(III) chain, collagen alpha-2(I) chain,
123 collagen alpha-3(VI) chain, and fibrillin-1. Additionally, essential cell-binding proteins such as
124 fibronectin were detected, although at reduced abundance. All three independently produced
125 Amniogel batches exhibited highly similar ECM protein profiles, demonstrating robust batch-to-
126 batch reproducibility. (Fig.1F).

127 Amniogels were formulated with ECM concentrations of 2.5–10 mg/ml. Formulations at 5–
128 10 mg/mL exhibited enhanced structural rigidity, facilitating easy handling and manipulation with
129 forceps (Fig.1G). SEM analysis of Amniogels revealed an inverse relationship between ECM
130 concentration in hydrogel and pore size (0.5712 ± 0.3099 µm at 2.5 mg/mL vs 0.1845 ± 0.08926
131 µm at 10 mg/mL; Fig. 1H, I). The 5 mg/mL concentration was selected for subsequent experiments
132 due to its optimal balance between handling properties and a pore size that favors the diffusion of

oxygen and nutrients. TEM further confirmed that collagen fiber integrity was preserved compared to native hAM (Fig. 1J).

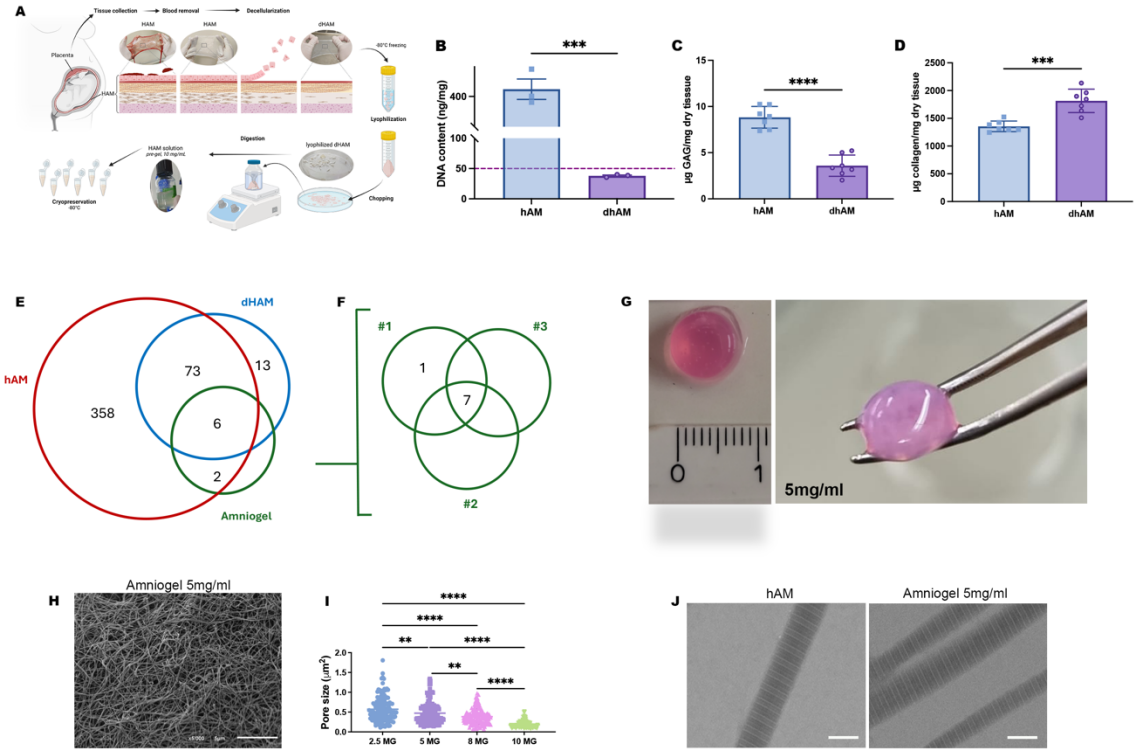

Figure 1 Generation and characterization of Amniogel (A) Schematic representation of Amniogel preparation. (B) DNA quantification in fresh (hAM) and decellularized (dHAM) human amniotic membranes. Data are presented as mean ± SD, two-tailed unpaired t-test, ***p = 0.0003 (n = 3 biological replicates). (C, D) Quantification of collagen, and GAGs. Data are presented as mean ± SD, two-tailed unpaired t-test, ****p <0.0001, ***p = 0.0002 (n = 7 biological replicates). (E, F) Comparative analysis of ECM protein retention across fresh hAM, dHAM and Amniogel. Venn diagram highlights 92 proteins retained post-decellularization, with six proteins shared across all conditions. Pepsin digestion of dHAM revealed retention of eight proteins, including Collagen alpha-1(I), Collagen alpha-2(I), Collagen alpha-3(IV), and Fibrillin-1. The

144 reproducibility of Amniogel protein composition was confirmed across three independent batches,
145 with six proteins consistently retained across all batches and one protein identified in individual
146 batches. (G) Macroscopic view of Amniogel at 5 mg/ml. (H) SEM images of Amniogel (5 mg/ml)
147 displaying an interconnected fibrous network. Scale bars, 5 µm. (I) Pore size analysis of Amniogel.
148 A progressive reduction in pore size was observed between 2.5 and 5 mg/mL, with a pronounced
149 decrease at 8 and 10 mg/mL. Data are presented as mean ± SD, one-way ANOVA with Tukey's
150 correction: 2.5 mg/ml vs. 5 mg/ml, **p=0.0025; 2.5 mg/ml vs. 8 mg/ml, ****p<0.0001; 2.5
151 mg/ml vs. 10 mg/ml,****p <0.0001; 5 mg/ml vs. 8 mg/ml, **p=0.0097; 5 mg/ml vs. 10 mg/ml
152 ****p<0.0001; 8 mg/ml vs. 10 mg/ml, ****p<0.0001. Depicted are the mean values of 138
153 detected pores from six random areas per sample (n = 3 biological replicates). (J, K) TEM analysis
154 revealed no discernible differences in the fiber structure of collagen within Amniogel compared to
155 native human amniotic membrane (hAM). Scale bars, 500 nm.

156

157

158

159

160

161

162

163

164

165

166

167 Gelation kinetics of Amniogel were comparable to those of rat tail collagen type I (Fig. S1).
168 Amniogel demonstrated robust cytocompatibility and the capacity for cell-driven remodeling.
169 Our observations show that Amniogel contraction is influenced by both the concentration of
170 decellularized hAM and the cell seeding density. Specifically, when seeded with BOECs, gels with
171 lower stiffness (5 mg/mL) contracted to 37% of their initial area, while stiffer 8 mg/mL gels
172 retained 96% of their original dimensions (Fig. S2A, B). Over seven days, BOECs in 5 mg/mL
173 gels progressively reorganized into interconnected capillary-like networks, whereas 8 mg/mL gels
174 restricted morphogenesis to fragmented, short structures (Fig. S2C). This suggests that Amniogel
175 at 5 mg/mL provides an optimal balance of stiffness, enabling matrix remodeling and supporting
176 reproducible vessel formation.
177 Furthermore, BOECs cultured on Amniogel-coated plates showed a significant increase in cell
178 numbers relative to collagen controls, adopting spindle-shaped morphologies and proliferating
179 over seven days (Fig. S3A, B). Viability (FDA/PI) assays confirmed minimal cytotoxicity, with
180 >90% cell survival across all conditions, validating Amniogel's biocompatibility (Fig. S3C).
181 These results demonstrate that Amniogel is a biocompatible scaffold that retains essential ECM
182 components crucial for islet viability and function, while supporting cell attachment and matrix
183 remodeling.
184

185 **Islet survival and function in Amniogel**

186 We next evaluated whether Amniogel encapsulation protects and improves islet function. Under
187 normoxic conditions (20% O_2), viability of rat islets embedded in Amniogel was similar to controls
188 cultured in suspension (Fig. S4A, C, E). However, suspension-cultured islets formed clumps and
189 developed necrotic cores over time. Under hypoxic conditions (1% O_2 for 16 h), suspended islets

showed extensive necrosis, while Amniogel-embedded islets maintained high viability (Fig. S4B to E). Notably, Amniogel-embedded islets demonstrated significantly enhanced glucose-stimulated insulin secretion and a higher stimulation index (SI: 0.7 ± 0.3 vs 2.3 ± 0.95, $p = 0.05$) compared to hypoxic controls (Fig. S4F). These results suggest that Amniogel attenuates hypoxic injury and preserves islet functionality under stress.

To evaluate the impact of cellular adhesion to Amniogel on human β-cell function and viability, human islets were embedded in Amniogel to form endocrine constructs (hEC) or maintained in standard suspension culture (HI alone) as controls for 7 days. Islets embedded in Amniogel retained their normal morphology and hormone expression (Fig. 2A,B). Basal insulin release was reduced in hECs, suggesting improved glucose regulation (Fig. S5A). Furthermore, hECs showed significantly enhanced insulin secretion both under high-glucose stimulation (SI: 2.317 ± 0.195 vs 1.204 ± 1.135, $p = 0.0012$) and theophylline stimulation (SI: 4.240 ± 0.673 vs 2.385 ± 0.110, $p = 0.0092$) compared to HI alone (Fig. S5B, C). To elucidate mechanisms underlying enhanced insulin secretion in hECs, we analyzed β1-integrin expression. Immunofluorescence revealed a significantly increased β1-integrin expression in Amniogel-embedded islets compared to controls (Fig. 2C, D). This was confirmed by qPCR, showing a threefold increase in *ITGB1* expression ($p= 0.0016$; Fig. 2E). The elevated β1-integrin expression was associated with significantly reduced pro-apoptotic *CASP3* expression ($p = 0.0003$) and increased anti-apoptotic *BCL2* expression by a 4.8-fold ($p=0.0089$; Fig. 2F, G).

These findings demonstrate that Amniogel promotes β-cell viability, structural integrity, and insulin secretion by enhancing cellular interactions and reducing apoptosis.

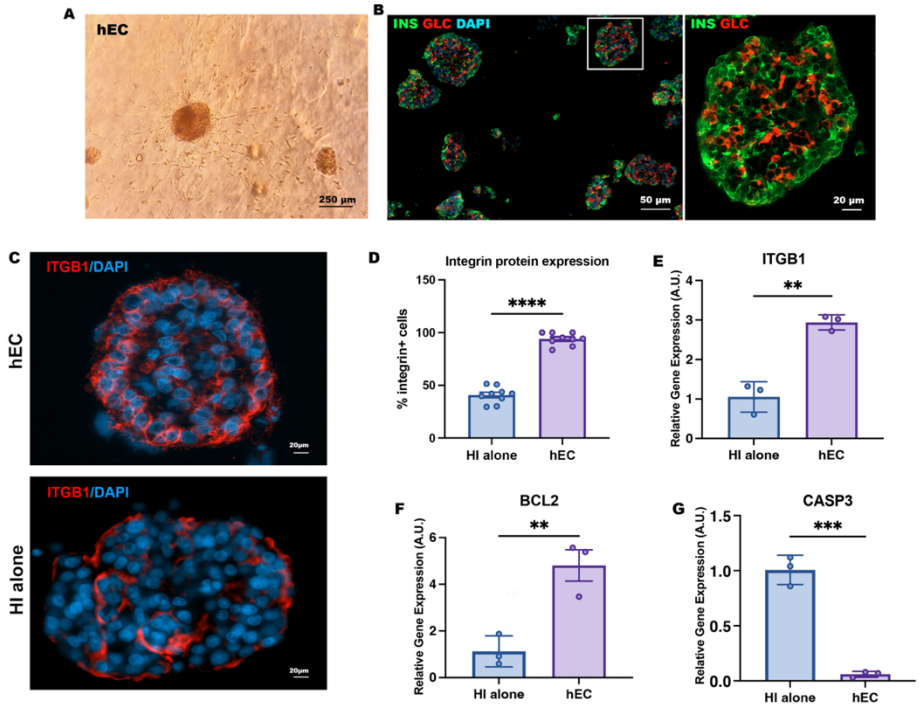

Figure 2 Amniogel Enhances Human Islet Viability and Function (A, B) Optical microscopy and immunofluorescent images of Amniogel-embedded human islets cultured for 7 days. Islets were stained for insulin (green) and glucagon (red). (C–D) Representative immunofluorescence images and quantification of β1-integrin expression in hECs and human islets in suspension. Data are presented as mean ± SD, two-tailed unpaired t-test, ****$p < 0.0001$. (E) qPCR analysis revealed a threefold upregulation of ITGB1 mRNA in the hEC group, consistent with enhanced β1-integrin protein expression. Data are presented as arbitrary units (AU) after normalization to housekeeping genes, mean ± SD, two-tailed unpaired t-test, **$p = 0.0016$ ($n = 3$ biological replicates). (F, G) Gene expression analysis revealed reduced expression of the pro-apoptotic marker CASP3 and a significant increase in the anti-apoptotic marker BCL2 in the hECs. Data are presented as arbitrary units (AU) after normalization to housekeeping genes, mean ± SD, two-tailed unpaired t-test, **$p = 0.0089$, ***$p = 0.0003$ ($n = 3$ biological replicates).

Amniogel supports endothelial cell self-organization into a vascular network

To evaluate Amniogel's ability to support endothelial cell self-organization, LV-GFP BOECs were embedded in Amniogel and cultured in vasculogenic media (VM) (Fig. 3A).

Cells formed interconnected structures within 48 hours, evolving into a robust vascular network by day 7 (Fig. 3B). Individual cells were no longer distinguishable, indicating their complete integration into continuous tubular structures (Fig. 3C). Functional validation was demonstrated by Texas red–labeled dextran perfusion into hollow lumens, confirming effective fluid transport (Fig. 3D). Immunostaining further demonstrated that the vessel-like structures were surrounded by a basement membrane, as evidenced by collagen type IV deposition (Fig. 3E). These findings indicate that Amniogel provides a supportive microenvironment facilitating endothelial cell self-organization into functional vascular networks.

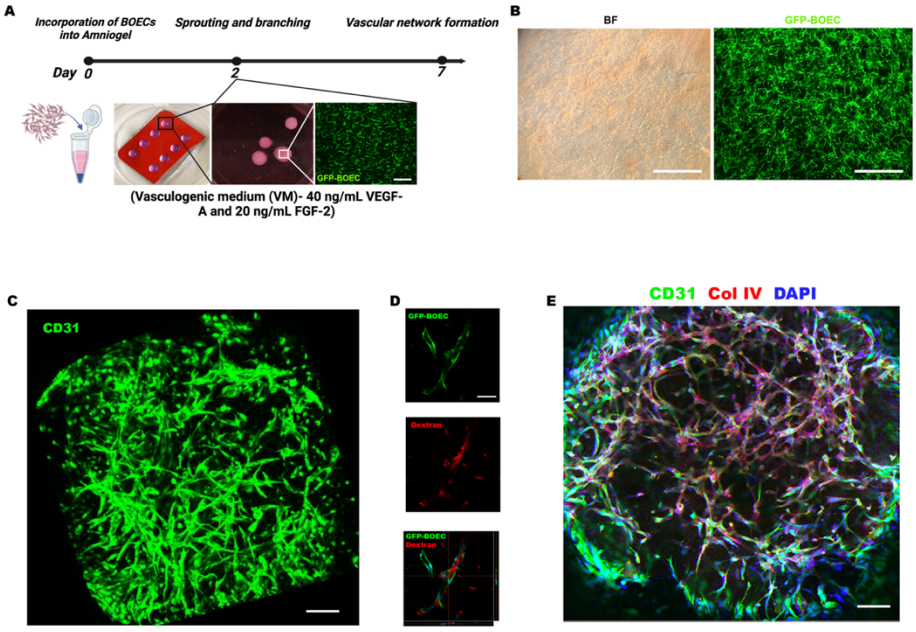

Figure 3 Amniogel Facilitates Formation of vascular networks. (A) Schematic representation of vascular construct generation. Scale bars, 500 µm. Created in https://BioRender.com (B) Representative bright-field and immunofluorescence images of LV-GFP transduced BOECs

255 showing the establishment of vascular networks. Scale bars, 500 μm. (C) 3D reconstruction of
256 capillary organization (CD31, green) in a vascular construct. Scale bars, 50 μm. (D) Formation of
257 hollow endothelial structures within 3D constructs, visualized through virtual stacks of LV-GFP
258 transduced BOECs incubated with Texas Red-labeled dextran. Scale bars, 30 μm. (E) Whole-
259 mount immunofluorescence of vascular networks showing endothelial cells (CD31, green) and the
260 vascular basement membrane (Col IV, red). Scale bars, 50 μm.

261

262

263 **Generation of vascularized endocrine constructs**

264 We hypothesized that Amniogel could facilitate the synergistic interaction between endothelial
265 cells and pancreatic islets, thereby supporting the development of more complex vascularized
266 endocrine constructs (hVECs). To test this hypothesis, we incorporated both human derived islets
267 and BOECs into Amniogel and cultured them for 7 days in optimized vasculogenic medium
268 (OVM) (Fig. 4 A). Within 3 days, BOECs formed continuous 3D vascular networks around islets
269 (Fig. 4B). Interestingly, despite the initial lack of laminin in Amniogel, the islets were surrounded
270 by a laminin-rich matrix (Fig. 4C). qPCR analysis identified BOECs as the primary laminin source,
271 showing a 3.9-fold increase in *LAMB1* expression in hVECs (p=0.008) and 5.7-fold in BOECs
272 (p=0.0003) versus HI alone (Fig. 4D). This indicates that BOECs play a critical role in laminin
273 deposition within the gel, leading to the development of a physiological-like ECM surrounding the
274 islets.

275 To explore functional implications of vascular integration, we investigated the role of gap
276 junctions, specialized membrane domains composed of nonspecific channels that facilitate cell-to-

277 cell communication, which is essential for coordinated insulin release (Fig. 5A) (*37*). qPCR
278 analysis revealed significant upregulation of *GJD2,* with increases observed in both hECs and
279 hVECs (5.3-fold, $p = 0.0057$, and 8.8-fold, $p < 0.0001$, respectively) compared to HI alone (Fig.
280 5B). Similarly, expression of *GJA1* increased notably, rising 6.3-fold in hECs ($p = 0.0042$) and
281 11.4-fold in hVECs ($p< 0.0001$) relative to controls (Fig. 5C), indicating strong coupling between
282 β cells and endothelial cells. Consistent with these molecular findings, functional glucose-
283 stimulated insulin secretion (GSIS) assays showed superior performance in vascularized
284 constructs, characterized by reduced basal secretion and increased glucose responsiveness (Fig.
285 S6). Together, these data suggest engineered vasculature within Amniogel enhances islet function
286 through dual mechanisms: (i) BOEC-derived laminin deposition recapitulating native peri-islet
287 ECM, and (ii) connexin-mediated cell–cell communication essential for coordinated insulin
288 release.
289
290
291

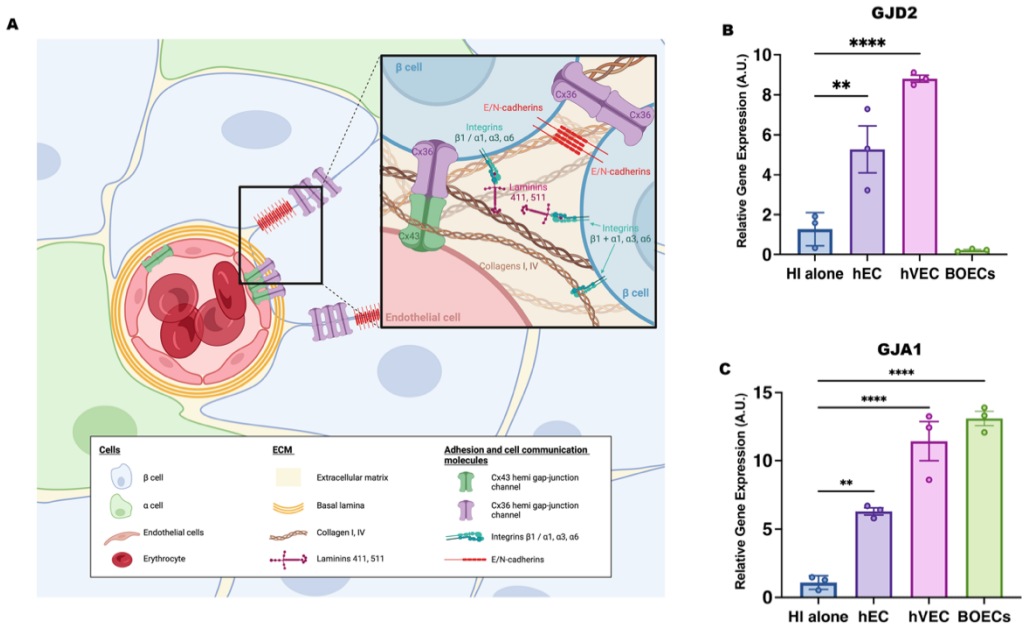

Figure 4 Engineering vasculature within amniogel promotes islet intercellular and cell-to-matrix communication. **(A)** Graphical illustration of known intercellular and ECM–cell interactions within islets. Cell adhesion molecules enhance β-cell glucose responsiveness, while connexin 36 and connexins 36/43 mediate insulin release by coordinating communication between β-cells and endothelial cells. Cadherins support cell–cell adhesion and inhibit apoptosis in α and β- cells. The ECM, enriched with laminin-211, laminin-511, and type IV collagen, forms a microenvironment that promotes granule secretion, cell proliferation, and apoptosis inhibition. Integrins bind ECM components like collagen and laminin, activating signaling cascades that regulate cell survival, growth, and differentiation. Created in https://BioRender.com (B) qPCR analysis revealed a 5.3-fold upregulation of GJD2 mRNA in hECs and an 8.80-fold upregulation in hVECs compared to HI alone. Data are presented as arbitrary units (AU), normalized to housekeeping genes, and shown as mean ± SD. One-way ANOVA with Tukey's correction, hEC vs HI alone, **p = 0.0057; hVEC vs HI alone, ****p<0.0001; HI alone vs BOECs, n.s. p= 0.5452 (n = 3 biological replicates). (C) qPCR analysis demonstrated a 6.3-fold upregulation of GJA1

315 mRNA in hECs and an 11.4-fold upregulation in hVECs compared to HI alone. Data are presented
316 as AU, normalized to housekeeping genes, and shown as mean ± SD, one-way ANOVA with
317 Tukey's correction, hEC vs HI alone, **p = 0.0042; hVEC vs HI alone, **** p<0.0001; HI alone
318 vs BOECs, **** p<0.0001 (n = 3 biological replicates).
319
320
321 **In vivo biocompatibility**
322 To determine whether Amniogel triggers an immune response upon transplantation, empty
323 hydrogels were transplanted subcutaneously into immunocompetent C57BL/6 mice (Fig. S7A).
324 Grafts were harvested 1month post-implantation and analyzed histologically. H&E staining
325 revealed modest mononuclear cell infiltration at the implantation sites without granuloma
326 formation, indicating minimal local toxicity and high tissue compatibility (Fig. S7B). Masson's
327 trichrome staining demonstrated preserved collagen fibrils in the Amniogel. Spindle-shaped cells,
328 likely fibroblasts, were also observed within the grafts. Immunohistochemical staining for CD45
329 and CD11b confirmed that immune cell infiltration in transplanted acellular gels was comparable
330 to that in sham-operated controls (Fig. S7B).
331 **Site-specific engraftment of non-vascularized endocrine constructs**
332 We then tested the performance of the Amniogel-based constructs in vivo using streptozotocin-
333 diabetic NSG immunodeficient mice (Fig. 5A). In the highly vascularized epididymal fat pad
334 (EFP) site, even non-vascularized endocrine constructs (EFP-rEC) significantly outperformed islet
335 transplanted alone (EFP-rI). All mice receiving EFP-rECs achieved normoglycemia within one
336 week, whereas only ~55% in the EFP-rI group became normoglycemic (Fig. 5B, C). An
337 intraperitoneal glucose tolerance test (IPGTT) at 5 weeks post-transplant showed that EFP-rEC

338 recipients cleared glucose almost as efficiently as healthy nondiabetic mice, whereas EFP-rI mice
339 displayed impaired glucose tolerance (Fig. 5D, E). Removing the graft-bearing EFP led to
340 recurrence of hyperglycemia in cured mice, confirming that the implanted constructs were
341 responsible for diabetes reversal. Histological analysis at 14 weeks showed well-preserved islets
342 in the EFP-rEC grafts, with a larger insulin-positive area compared to islet-alone grafts (Fig. 5F,
343 G). Immunohistochemical staining for CD31 revealed a markedly higher vessel density in EFP-
344 rEC samples compared to controls (Fig. 5F, H), suggesting enhanced vascularization and
345 engraftment.
346 Despite these encouraging results, the subsequent subcutaneous transplantation of non-
347 vascularized endocrine constructs (SQ-rEC) proved unsuccessful. None of the recipients achieved
348 normoglycemia, demonstrating that simply providing an ECM scaffold was insufficient to support
349 islet function in this poorly vascularized environment (Fig. S8). These findings confirmed that
350 prevascularization is essential for graft survival and efficacy in poorly vascularized subcutaneous
351 site.
352

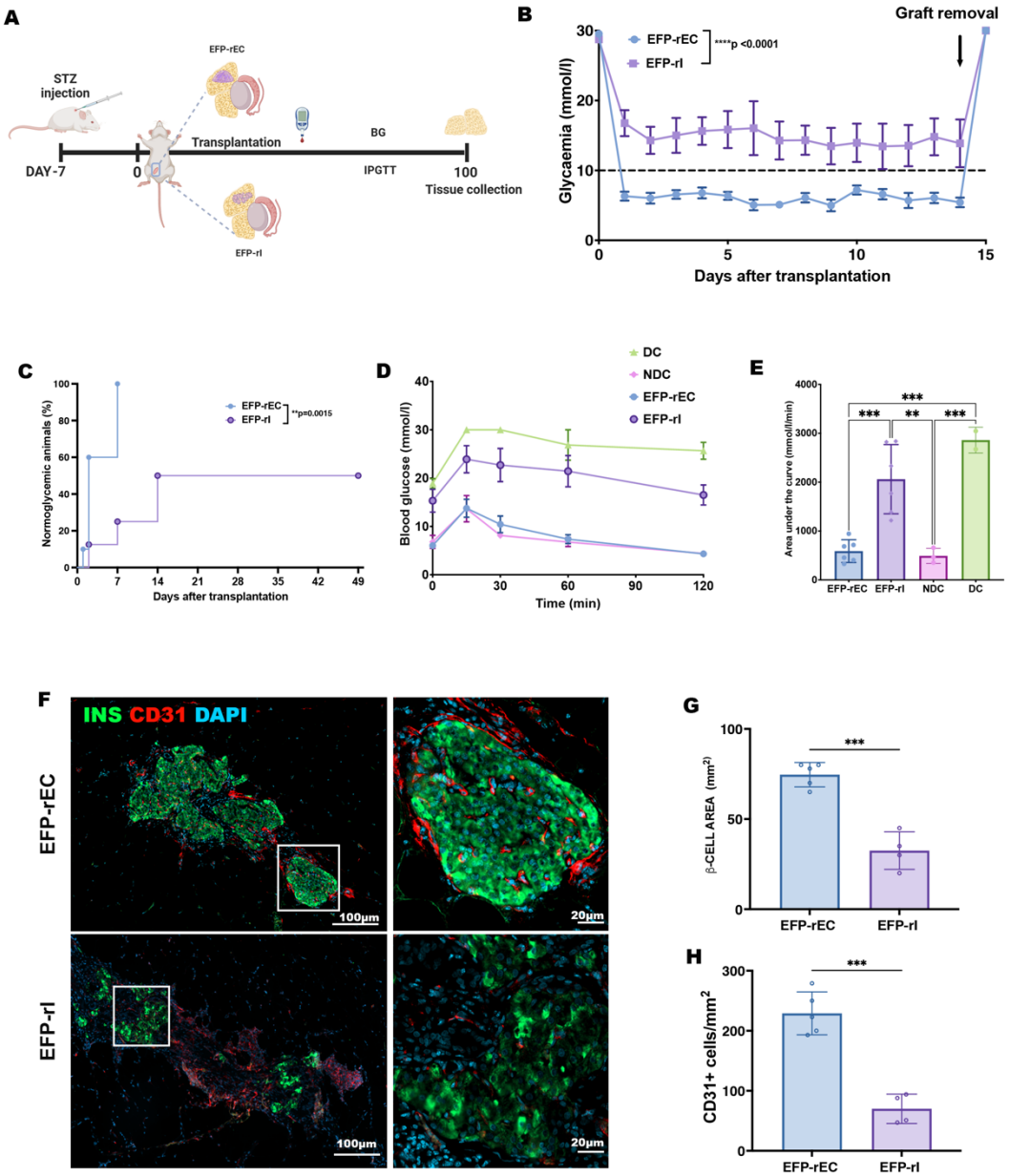

Figure 5 Function of endocrine constructs transplanted in EFP. (A) Schematic representation of the experimental setup. (B) Blood glucose measurements following transplantation. Grafts were removed on day 100 (indicated by arrow). Data are presented as mean ± SEM, analyzed by two-way ANOVA with Sidak correction, ****$p < 0.0001$. (C) Kaplan-Meier analysis of the percentage of mice achieving normoglycemia (≤11 mmol/L). Differences between EFP-rEC and EFP-rI groups were assessed using a two-sided log-rank (Mantel–Cox) test, **$p = 0.0015$. (D) Blood

370 glucose curves from the IPGTT on day 30 for EFP-rEC (n = 6), EFP-rI (n = 6), non-diabetic healthy
371 controls (NDC, n = 3), and diabetic controls (DC, n = 2). Data are presented as mean ± SEM. (E)
372 AUC analysis of IPGTT on day 30 for EFP-rEC (n = 6), EFP-rI (n = 6), NDC (n = 3), and DC (n
373 = 2). Data are presented as mean ± SD, analyzed by one-way ANOVA with Tukey's correction:
374 EFP-rEC vs. EFP-rI, ***p = 0.0006; EFP-rEC vs. DC, ***p = 0.0003; EFP-rI vs. NDC, **p =
375 0.0021. (F) Immunohistochemical staining of retrieved constructs on day 100 showing insulin
376 (green) expression and vascularization (CD31, red). (F) Representative immunofluorescent images
377 of rat insulin (green) and mouse blood vessels (CD31, red) in a retrieved constructs on day 100.
378 (G) Percentage of insulin-positive area in EFP-rEC (n=5) and EFP-rI (n=4) visualized 100 days
379 after transplantation. Data are presented as mean ± SD, two-tailed unpaired t-test, ***p=0.0002
380 (H) Blood vessel density in the EFP-rEC (n=5) and EFP-rI (n=4); Data are presented as mean ±
381 SD, two-tailed unpaired t-test, ****p=0.0001.
382

383 **Vascularized endocrine constructs improve glycemic control in subcutaneous transplants**

384 Building on *in vitro* findings demonstrating Amniogel's capacity to support vascular network
385 formation and enhance islet function through intercellular and cell-to-matrix communication, we
386 moved forward to evaluate the in vivo functionality of VECs in a clinically relevant but poorly
387 vascularized subcutaneous site.

388 To this end, the vascularized constructs (SQ-rVEC), were implanted subcutaneously in diabetic
389 NSG mice. For comparison, two additional groups of mice were transplanted with non-
390 vascularized constructs containing islets (SQ-rEC) or with islets alone (SQ-rI). Graft function was
391 monitored for 14 weeks (Fig. 6A). Remarkably, 96% of SQ-rVEC recipients achieved rapid
392 normoglycemia within one week, maintaining stable glucose levels significantly lower than both

control groups (p<0.001) (Fig. 6B, C). Glucose tolerance tests at day 30 showed that SQ-rVEC group responded to the glucose challenge similarly to healthy controls and significantly better than the SQ-rEC and SQ-rI groups (Fig. 6D, E).

Graft excision led to diabetes recurrence, confirming graft function. Histological analysis revealed well-vascularized, healthy islets in SQ-rVECs, contrasting with the smaller, fragmented, and poorly vascularized islets in SQ-rECs (Figure 6G). Notably, the implanted matrix remained intact and was repopulated by host cells in both groups. Quantification of blood vessels within and surrounding the constructs (Figure 6H).

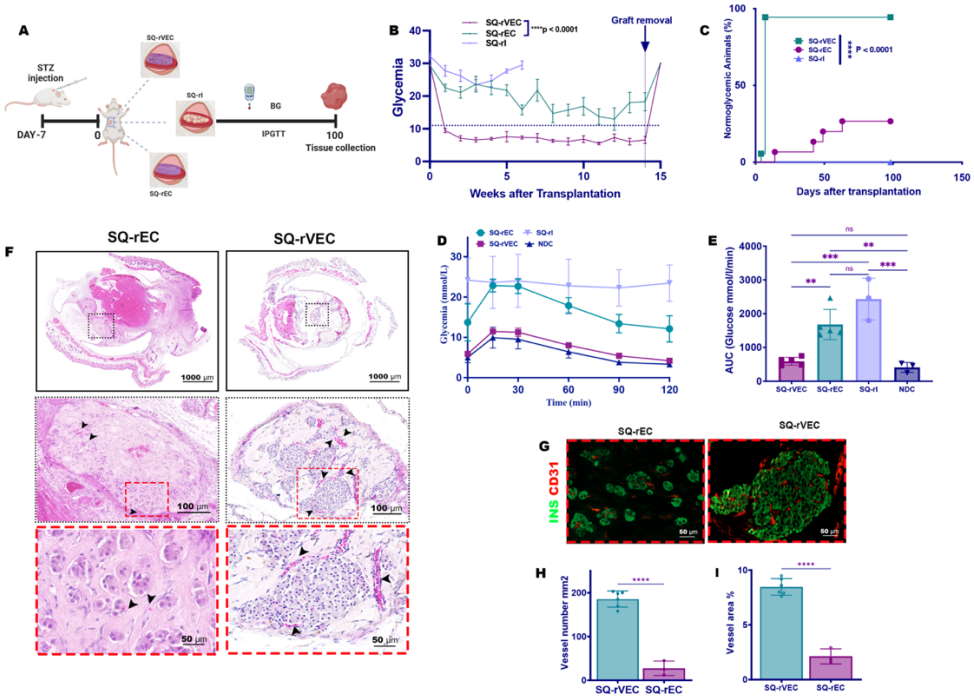

Figure 6 Performance of rat derived VECs after subcutaneous transplantation in diabetic mice. (A) Schematic representation of the experimental setup. (B) Blood glucose measurements following transplantation. Data are presented as mean ± SEM, analyzed by two-way ANOVA with Sidak correction, ****p < 0.0001. (C) Kaplan-Meier analysis of the percentage of mice achieving

normoglycemia (≤11 mmol/L). Differences between SQ-rVEC, SQ-rEC and SQ-rI groups were assessed using a two-sided log-rank (Mantel–Cox) test, ****p = 0.0001. (D) Graft function evaluated by IPGTT on day 30 for SQ-rVEC (n = 5), SQ-rVEC (n = 5), SQ-rI (n = 3) and NDC (n = 3). Data are presented as mean ± SEM (E) AUC analysis of IPGTT. Data are presented as mean ± SD, one-way ANOVA with Tukey's correction, SQ-rVEC v.s. SQ-rI, ***p=0.0001, SQ-rVEC vs. SQ-rEC, **p=0.0028; SQ-rVEC vs. NDC, n.s. 0.9101; SQ-rI vs. SQ-rEC, n.s. p=0.0700; SQ-rI vs. NDC, ***p=0.0001; SQ-rEC vs. NDC, **p=0.0026; (F) H&E-staining of retrieved constructs on day 100. Black arrowheads indicate blood vessels containing RBCs**;** (G) Immunohistochemical staining of retrieved constructs on day 100 showing insulin (green) expression and vascularization (CD31, red). (H, I) Blood vessel density and area percentage in the SQ-rVEC (n=6) and SQ-rEC (n=3); Data are presented as mean ± SD, two-tailed unpaired t-test, ****p<0.0001.

429 To evaluate clinical potential, we assessed subcutaneous transplantation of human islets. Given
430 mice's inherent resistance to human insulin and the requirement for a larger islet mass to achieve
431 normoglycemia in xenotransplantation studies (*38-44*), two islet-laden vascularized constructs
432 (SQ-hVEC) were implanted bilaterally into the ventral subcutaneous space. Control mice received
433 equivalent non-vascularized endocrine constructs (SQ-hEC). To minimize graft loss resulting from
434 innate immune responses known to occur even in severely immunodeficient mice (*45-47*),
435 experiments were limited to 45 days. This timeframe is clinically relevant, as islet function at one
436 month, assessed by the BETA-2 score (*48*), reliably predicts long-term transplant success (*49*).
437 SQ-hVEC group demonstrated superior outcomes, with 89% (8/9) achieving normoglycemia
438 within 14 days versus 33% (2/6) in SQ-hEC group (Fig. 7A, B). Human C-peptide levels correlated
439 with glycemic control (Fig. 7C), and glucose tolerance tests showed significantly improved
440 glucose clearance in SQ-hVEC mice (p=0.0057, Fig. 7D). All reverted to hyperglycemia upon
441 graft removal, confirming therapeutic dependence.
442 Explanted constructs showed clear differences between the two experimental groups. SQ-hVECs
443 were fully integrated with surrounding tissues and displayed well-defined, blood-perfused vascular
444 structures of various calibers surrounding the graft (Figure 7E). In contrast, SQ-hECs displayed
445 reduced vascularization and less effective integration with host tissues (Figure 7F). Histological
446 analysis showed viable islets with normal morphology in both groups (Figure 7 G, H). However,
447 islets in the SQ-hVEC group were surrounded by significantly more blood vessels than those in
448 the SQ-hEC group, consistent with the observed improvements in diabetes correction (Figure 7I).
449 Immunostaining for human and mouse CD31 demonstrated the presence of chimeric blood vessels,
450 indicating anastomoses and vascular remodeling (Figure 7J). Functional maturity of the
451 vasculature was confirmed by vessels with lumens containing erythrocytes, positively stained for

human CD31 and α-SMA (Figure 7K). Additionally, islets in the SQ-hVEC group regained laminin expression, an important extracellular matrix protein primarily deposited by endothelial cells (Figure 7L). Laminin was observed both within the islets and in the surrounding tissue. These findings demonstrate that prevascularizing Amniogel-based endocrine constructs significantly enhances islet engraftment and function in subcutaneous transplantation sites, leading to superior glycemic control.

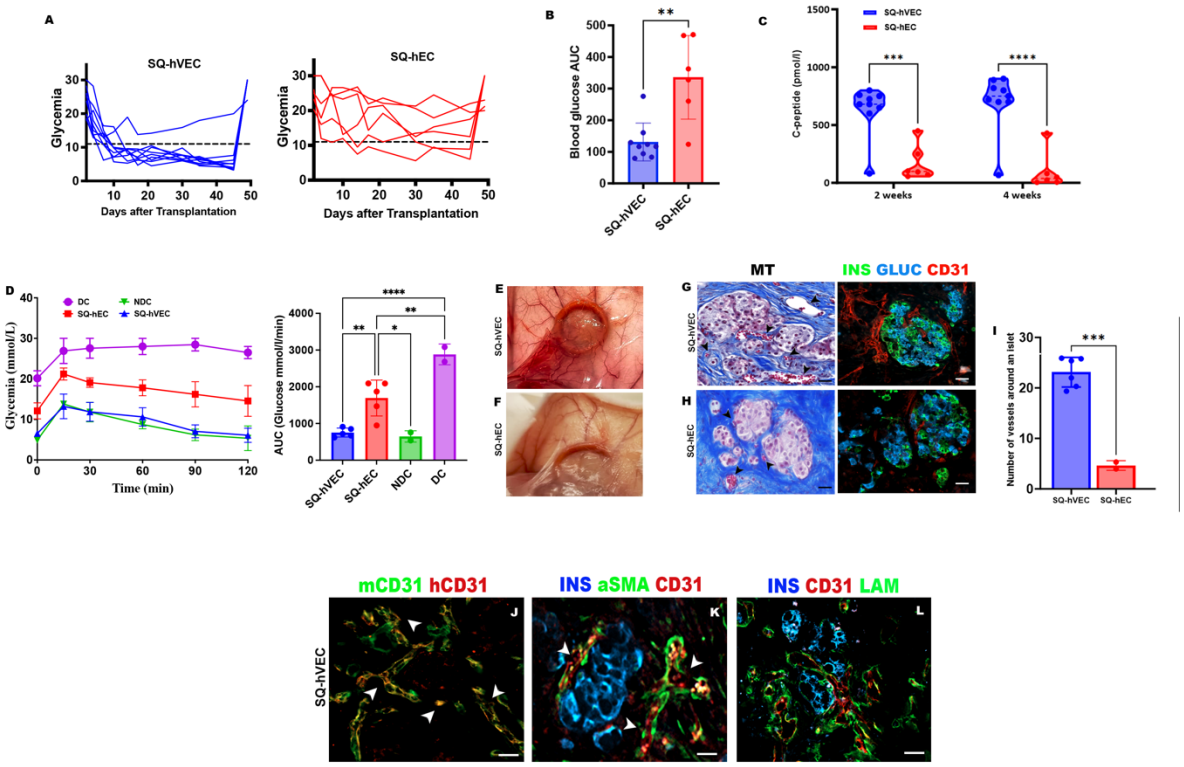

Figure 7 Performance of human VECs after subcutaneous transplantation in diabetic mice (A) Blood glucose measurements following transplantation. Data are presented as mean ± SEM, one-way ANOVA, SQ-hVEC vs. SQ-hEC, ****$p < 0.0001$; (B) AUC of blood glucose levels from day −7 to day 30. Data are presented as mean ± SD, Unpaired t-test, p**=0.0012. (C) IPGTT

463 results for SQ-hVEC (n = 5), SQ-hEC (n = 5), diabetic control (DC, n = 2), and non-diabetic
464 control (NDC, n = 2). Data are presented as mean ± SEM. (D) AUC analysis of IPGTT. Data are
465 presented as mean ± SD, one-way ANOVA with Tukey's correction, SQ-hVEC vs. SQ-hEC., **
466 p =0.0057, SQ-hVEC vs. NDC, n.s., p=0.9803, SQ-rVEC vs. DC, p****<0.0001, SQ-hEC vs.
467 NDC, p*=0.0168, SQ-hEC vs. DC, p**=0.0077 (E,F) Explanted constructs 45 days after
468 transplant. (G, H) Cross-sectional images of retrieved constructs on day 45 showing
469 insulin/glucagon-positive islets and vascularization of the graft. Masson's trichrome staining and
470 fluorescence immunohistochemistry with CD31 (red) revealed blood vessels containing RBCs
471 (black arrowheads (I) Blood vessel density in retrieved SQ-hVEC and SQ-hEC. Data are presented
472 as mean ± SD, two-tailed unpaired t-test, ***p=0.0002. (J-L) Immunofluorescent staining of SQ-
473 hVECs for insulin (blue), human CD31 (red), mouse CD31 (green), α-SMA (green), and laminin
474 (green). Chimeric blood vessels and mature vessels containing RBCs are indicated by white
475 arrowheads. Scale bars, 20 μm.

476
477
478
479
480
481
482
483
484
485
486 **DISCUSSION**

487 Recapitulating the key elements of the pancreatic niche, specificaly the ECM microenvironment
488 and vascular network is fundamental requirement for bioengineering a functional endocrine
489 pancreas (*50, 51*). While, collagen-based hydrogels and decellularized ECM matrices support
490 cellular integration and vascularization (*19, 30, 31, 52-58*), the scarcity of human ECM (*59, 60*),
491 its compromised structural integrity and cytotoxic residues associated with conventional detergent-
492 based decellularization techniques (*61, 62*) hinder clinical translation of these strategies.
493 In this study, we developed, Amniogel, a human amniotic membrane-derived hydrogel, that meets
494 these requirements. By mimicking the ECM and supporting vascularization, Amniogel recreates
495 an islet-like microenvironment. Our bioengineered endocrine constructs incorporate a collagen-
496 rich, biocompatible matrix reminiscent of the native islet niche (*63, 64*), and built-in dense, stable
497 capillary network directly interfaced with the encapsulated islets, enabling efficient glucose
498 sensing and insulin release even in the traditionally poor subcutaneous site.
499 From a translational perspective, the use of Amniogel platform offers several key advantages.
500 Amniotic membrane is an ethically sourced, established, FDA-approved clinical-grade material
501 widely used in in wound healing and ophthalmology (*65-69*). Our GMP-compliant manufacturing
502 protocol is scalable and reproducible. All reagents used in Amniogel production are available in
503 clinical-grade formulations. Additionally, its cost-effective production provides a viable
504 alternative to expensive purified ECM components. Beyond its biochemical composition,
505 Amniogel demonstrates optimal self-assembly, structural integrity supporting cell adhesion and
506 proliferation, and robust biocompatibility in immunocompetent hosts. Utilization of the host-
507 derived endothelial for vascularization is another important factor to facilitate clinical translation.
508 Taken together, these features give Amniogel a significant regulatory advantage by capitalizing
509 on existing approval frameworks rather than requiring entirely new pathways (*70*).

510 A central finding of our work is that providing an appropriate human ECM substrate significantly
511 boosts islet graft health by engaging cell–matrix survival pathways. Isolation procedures often
512 disrupt the islet ECM, triggering β-cell apoptosis via β1-integrin signaling (*71*). Previous studies
513 have demonstrated supplementing ECM proteins improves islet survival and function (*72*). In line
514 with these observations, our results showed that islets embedded in Amniogel exhibited improved
515 glucose-responsive insulin secretion and increased expression of β1-integrin, a key mediator of
516 cell-ECM adhesion critical for β-cell survival. Additionally, Amniogel-embedded islets displayed
517 reduced pro-apoptotic CASP3 and elevated anti-apoptotic BCL2 expression. These findings
518 suggest that restoring cell–matrix interactions effectively reduce β-cell apoptosis, consistent with
519 the established role of β1-integrin signaling in promoting β-cell survival (*64, 73, 74*). Furthermore,
520 we observed enhanced intercellular communication in generated VECs, via connexin-mediated
521 gap junctions. Cx-36, predominantly expressed in β-cells and facilitates coordinated insulin release
522 (*37, 75*) while, Cx-43 mediates endothelial–β-cell communication, increasing islet size and insulin
523 content (*75-77*). Our results show significant upregulation *GJD2* (5.27-fold in Amniogel; 8.08-
524 fold in vascularized constructs) and *GJA1* (6.3-fold in Amniogel; 11.4-fold in vascularized
525 constructs) compared to suspension cultures, suggesting that matrix components enhance gap-
526 junctional intercellular communication. However, it remains unclear whether this effect is
527 specifically due to laminin or broader ECM-mediated mechanisms that stabilize islets. ECM–
528 integrin interactions strongly influence connexin expression and intercellular communication in
529 other cell types (*78, 79*), suggesting a similar mechanism in our observations. Given laminin's
530 known role in integrin activation and connexin regulation (*80-82*), β1-integrin signaling may
531 promote ECM-mediated gap junction formation, thus enhancing synchronized insulin secretion in
532 β-cells. These molecular changes were associated with decreased basal insulin secretion and

533 improved glucose responsiveness in vascularized constructs, further supporting the ECM's
534 functional relevance in β-cell physiology. Additional studies are required to elucidate the precise
535 contribution of laminin–integrin signaling to gap junction assembly and to clarify whether these
536 effects arise primarily from BOEC interactions, β1-integrin signaling, or both.
537 The development of functional 3D vascular networks remains a critical hurdle in tissue engineering
538 (*83*). Amniogel promotes endothelial cell self-assembly into interconnected vascular structures,
539 creating a microenvironment conducive to sustained nutrient and oxygen delivery to encapsulated
540 islets. This spatial arrangement ensures insulin secretion occurs near blood vessels, a prerequisite
541 for optimal graft function in poorly vascularized transplant sites. Furthermore, utilization of
542 BOECs, which can be derived from the recipients themselves is a key advantage of this approach.
543 Evidence shows that humoral immune responses significantly contribute to vascularized allograft
544 failure (*84, 85*), as donor-specific antibodies (DSA) primarily target the mismatched HLA
545 molecules, expressed on graft endothelial cells (*86*). Consequently, antibody-mediated rejection
546 (AMR) predominantly affects graft microvasculature (*87*). Experimental evidence further shows
547 that endothelial chimerism—where recipient-derived vessels vascularize the graft—confers
548 resistance to AMR (*86*). Moreover, recent studies indicate allogeneic graft endothelia are also
549 susceptible to innate immune attacks by recipient natural killer (NK) cells, causing antibody-
550 independent graft injury (*88-90*). Thus, replacing donor endothelial cells with autologous BOECs
551 represents a promising strategy to reduce immune activation and prolong graft survival.
552 Importantly, BOECs from both diabetic and non-diabetic patients have been shown to enhance
553 islet engraftment with equal efficacy (*91*), reinforcing their potential for clinical use. Their
554 accessibility, robust proliferative capacity, and intrinsic ability to form functional vascular
555 networks render them highly suitable for improving engineered tissue stability and function (*92,*

556 *93*). Our findings further demonstrate that BOEC-derived vasculature surrounding islets produces
557 a basement membrane-like ECM enriched in laminin, mimicking the native islet niche. This
558 observation aligns with previous reports that β-cells rely on intra-islet endothelial cells to
559 synthesize basement membrane constituents (*94*).

560 In vivo studies confirmed that both ECM and prevascularization are essential for optimal
561 engraftment of the engineered constructs. In a marginal islet transplant model within the highly
562 vascularized epididymal fat pad, Amniogel-embedded islets exhibited significantly improved
563 engraftment compared to islets transplanted alone. However, non-vascularized constructs at the
564 same islet dose failed to restore normoglycemia, likely due to insufficient oxygenation and nutrient
565 exchange in this poorly vascularized site. These findings align with previous reports indicating
566 that although ECM integration enhances cell survival, robust vascularization remains critical for
567 effective glucose sensing and insulin secretion, particularly in the subcutaneous space, which
568 remains challenging despite clinical benefits [33, 93]. This limitation was overcome by
569 preveascularizing subcutaneously implanted endocrine constructs, resulting in significantly
570 improved islet survival and function. Notably, 96% of SQ-rVEC recipients achieved
571 normoglycemia within one week, compared to 20% in the SQ-rEC group and none in the SQ-rI
572 group. Histological analysis confirmed increased vessel density in SQ-rVEC grafts, reinforcing
573 the crucial role of vascularization for successful engraftment. Replication of these experiments
574 with human islets yielded similar results, including rapid elevation of circulating human C-peptide
575 post-transplantation. Explanted human grafts displayed excellent islet morphology, hormone
576 expression and extensive vascularization. The presence of red blood cells and α-SMA-positive
577 vessels indicated functional maturity, while chimeric vessels and restored laminin expression
578 further confirmed successful vascular integration.

579 Taken together, these results demonstrate that vascularized endocrine constructs effectively
580 address the critical limitations associated with subcutaneous islet transplantation by facilitating
581 rapid vascular integration and sustaining islet function.
582 Beyond these advantages, the versatility of Amniogel opens opportunities for broader application
583 in regenerative medicine. the versatility of Amniogel broadens its potential in regenerative
584 medicine, making it suitable for stem cell-derived insulin-producing cells, xenogeneic islets, or
585 other therapeutic cell types. Additionally, Amniogel could be modified with immunomodulatory
586 cells or molecules to optimize the local immune microenvironment and enhance engraftment
587 outcomes. Nevertheless, any modifications must be carefully optimized to maintain the established
588 safety profile of amnion-derived products and avoid introducing additional regulatory
589 complexities (*95*).

590

591 **MATERIALS AND METHODS**

592

593 **Study Design**

594 The objective of this study was to develop a clinically scalable, vascularized endocrine construct
595 (VEC) using a human amniotic membrane–derived hydrogel for β-cell replacement therapy.
596 Amniogel was manufactured under GMP-compatible conditions and evaluated for ECM content,
597 gelation properties, and biocompatibility. Pancreatic islets, alone or co-encapsulated with blood
598 outgrowth endothelial cells (BOECs), were embedded in Amniogel and assessed for viability,
599 vascular network formation, and insulin secretion in vitro.
600 Therapeutic efficacy was tested in streptozotocin-induced diabetic NSG mice following
601 transplantation of constructs into the epididymal fat pad or subcutaneous space. Functional

602 outcomes included glycemic control, glucose tolerance, and histological evidence of engraftment
603 and vascular integration.
604 Sample size was determined using power analysis (G*Power). Randomization was performed after
605 diabetes induction, and group allocation was concealed during transplantation. Investigators
606 assessing outcomes were blinded to group assignments when feasible, and were independent from
607 those conducting the experiments.
608

609 **Amniogel Preparation**

610 To generate Amniogel in line with GMP for future clinical use, we formulated a precise five-step
611 protocol. The process includes the harvesting of tissue, decellularization, sterilization, freeze-
612 drying, mincing, digestion, purification and neutralization (Fig. 1A).
613 Immediately after delivery, placenta was immersed in sterile PBS supplemented with antibiotics
614 (100 U/ml penicillin, 100 mg/ml streptomycin, and 0.25 mg/ml amphotericin B) and transferred
615 to the laboratory. Under sterile conditions, the human amniotic membrane (hAM) was separated,
616 rinsed to remove blood clots, and decellularized using 10X TrypLE™ Select (ThermoFisher
617 Scientific) for 40 minutes at 37°C with shaking. Decellularized membranes were washed, freeze-
618 dried, minced, and digested with 1 mg/mL porcine pepsin (Sigma Aldrich) in 0.04 N HCl for 48
619 hours at room temperature. The solubilized hAM, rreferred to as "pre-gel" was centrifuged,
620 adjusted to 10 mg/mL, aliquoted, and stored at -80°C.
621 Gelation was achieved by neutralizing pre-gels (pH 7.4) with MCDB 131 medium and $NaHCO_3$,
622 yielding 8 mg/mL Amniogel. Neutralized gel (62%) was mixed with cell suspension (38%),
623 yielding hydrogels with 5 mg/mL matrix proteins, cast into silicon molds or droplets, and
624 polymerized at 37°C for 30 minutes.

625 Amniogel batches were assessed for DNA/protein content, gel formation, and biocompatibility.

626

627 **Evaluation of Amniogel's Impact on Islet Function**

628 Rat or human islets (1000 IEQ) were suspended in 100 μL of neutralized Amniogel, loaded into
629 silicone molds, and incubated at 37 °C to facilitate gelation. The gelled constructs were cultured
630 for 7 days, with the medium replaced every other day. Suspension-cultured islets served as
631 experimental controls.

632 To evaluate the potential cytoprotective effects of Amniogel on islet cells under ischemic
633 conditions, an experiment was conducted with two groups: islet cells embedded within Amniogel
634 and control islet cells cultured without the gel. Both groups were exposed to a 16-hour hypoxic
635 environment to simulate ischemia.

636 The experiment was performed in a humidified incubator connected to a nitrogen supply,
637 maintaining a gas mixture of 1% oxygen, 5% CO_2, and 94% nitrogen. This setup accurately
638 replicated the low-oxygen environment characteristic of ischemia. The incubator temperature was
639 consistently maintained at 37 °C throughout the experiment.

640 Static glucose-stimulated insulin secretion (GSIS) assays were conducted to assess function of
641 islets. To this end, islets embedded in Amniogels or maintained in suspension culture were
642 sequentially incubated in 2.8 mM glucose (basal) and 16.7 mM glucose (stimulated) for 1 h each,
643 and supernatants were collected for insulin quantification. Human islets underwent an additional
644 stimulation step using 5 mM theophylline to enhance insulin secretion. Total insulin content was
645 extracted using acid-ethanol, and the stimulation index (SI) (stimulated/basal insulin secretion)
646 was calculated. All assays were performed in duplicate with 100 IEQ per condition.

647 **Vascular network formation in Amniogel constructs**

648 GFP-labeled BOECs (2×10^6/mL) were mixed with Amniogel, dispensed into 10–15 µL droplets,
649 and incubated at 37°C with 5% CO_2 for 30 minutes. Gelled droplets were cultured in vasculogenic
650 media (VM) composed of complete EM supplemented with 40 ng/mL VEGF-A and 20 ng/mL
651 FGF-2 for 7–14 days.

652 **Assembly of vascularized endocrine constructs**

653 To study vascular network formation and islet vascularization, isolated islets (1000 IEQ) and
654 BOECs (2×10^6) were encapsulated in 100 µL of Amniogel. The mixture was cast into silicone
655 molds to form 10 µL droplets, polymerized, and cultured at 37 °C for 7 days in optimized
656 vasculogenic medium (OVM), a 1:1 mixture of complete DMEM and VM specifically formulated
657 to maintain islet and endothelial cell viability while promoting vascular network self-assembly.
658 Controls included free islets and islet-laden Amniogels cultured under the same conditions.

659 **Live Visualization**

660 To study endothelial self-organization and network formation, live microscopy was conducted
661 using an epifluorescent microscope (DMi8 manual microscope; Leica Microsystems, Heerbrugg,
662 Switzerland). This was done without additional staining, as the endothelial cells were labeled with
663 GFP. Observations were initiated 24 hours after casting the construct, allowing sufficient time for
664 polymerization and stabilization to occur within the construct.

665 **Lumen Formation Analysis and Immunofluorescence**

666 Free-floating constructs were fixed in 4% paraformaldehyde at room temperature for 2 hours and
667 blocked with 3% FBS, 1% BSA, 0.5% Triton X-100, and 0.5% Tween for 2 hours. Primary
668 antibodies against insulin (1:50, DakoCytomation) and CD31 (1:100, DAKO) were applied
669 overnight at 4°C, followed by secondary antibodies (donkey anti-guinea pig Alexa Fluor 488 and

670 donkey anti-mouse Alexa Fluor 594, both 1:500, Jackson ImmunoResearch) for 45 minutes and
671 three PBS washes.
672 To confirm lumen formation, constructs were incubated with 0.5 mg/mL Texas red-labeled
673 Dextran (10,000 MW, ThermoFisher) in MCDB 131 medium at 37°C and 5% CO_2 overnight, fixed
674 in 4% PFA for 30 minutes, and washed with PBS.
675 Samples were cleared with RapiClear overnight at room temperature and mounted in iSpacer
676 microchambers. Fluorescent imaging was performed using a Nikon A1R confocal microscope, and
677 Z-stacks were generated with NIS-Elements Imaging Software.
678 **Implantation of Endocrine Constructs into the Epididymal Fat Pad of Diabetic Mice**
679 Immediately after isolation, 250 rat IEQs were aliquoted into 38 µl of medium, combined with 62
680 µl of neutralized Amniogel, cast into 10 µL silicone elastomer molds, and polymerized at 37°C.
681 Constructs were cultured for 24 hours. On the day of transplantation, a 0.7 cm incision was made
682 in the peritoneal wall near the genital area to expose the EFP. The islet-laden Amniogels were
683 positioned on the fat pad, folded, and reinserted into the peritoneal cavity. Each mouse received
684 four endocrine constructs containing approximately 250 IEQ (EFP-rEC; n=8). Control mice were
685 transplanted with 250 IEQ alone (EFP-rI; n=8).
686 **Subcutaneous transplantation of vascularized endocrine constructs**
687 For subcutaneous transplantation, rat or human islets (1000 IEQ) were combined with BOECs (0.2
688 $\times 10^6$) and mixed with Amniogel. For human islets, 100 µL of the mixture was cast into 9 mm
689 silicone molds; for rat islets, 10–15 µL droplets were dispensed into silicone elastomer molds. The
690 polymerized constructs were cultured at 37°C in OVM overnight.
691 Next day, mice were anesthetized with 2.5% isoflurane, and a 0.5 cm incision was made to create
692 subcutaneous pockets. A silicone ring was placed on the muscle and secured with Tisseel fibrin

693 sealant (Baxter AG) to prevent migration. Constructs were inserted into the ring, and the incision
694 was sealed with Tisseel fibrin sealant and sutured using 5–0 silk.
695 For rat islet constructs (SQ-rVEC), mice (n=18) received 8–10 microgels containing 1000 islets
696 on the left side. Controls included non-vascularized endocrine constructs (SQ-rEC) with identical
697 islet quantities (n=15) and subcutaneously implanted naked islets (n=6).
698 For human islet constructs (SQ-hVEC; n=9), a single construct. (9mm diameter) containing 1000
699 IEQ was implanted on each side (2000 IEQ total). Mice transplanted with nonvascularized
700 constructs (SQ-hEC; n=6), containing equal number of islets served as controls.
701 **Histopathological analysis and immunostaining**
702 Explanted grafts were fixed in 4% paraformaldehyde and either paraffin-embedded or snap-frozen
703 in OCT compound (Tissue-Tek, Sakura Finetek). Serial 5 µm sections (10 per graft) were prepared
704 for hematoxylin-eosin (H&E), Mason Trichrome (MT), or immunofluorescence staining.
705 For immunostaining, sections were permeabilized, blocked, and incubated overnight with primary
706 antibodies against insulin (1:50, DakoCytomation), glucagon (1:4000, Sigma-Aldrich), human-
707 specific CD31 (1:50, DakoCytomation), CD31 (1:50, Abcam), CD34 (1:2000, Abcam), laminin
708 (1:30, Sigma-Aldrich), collagen IV (1:30, Bio-Rad), CD45 (1:100, Abcam), and CD11b (1:200,
709 Abcam). Secondary antibodies included goat anti-mouse, anti-rabbit, anti-guinea pig (1:300,
710 ThermoFisher Scientific), goat anti-guinea pig (1:500, Jackson ImmunoResearch), donkey anti-
711 rabbit Alexa Fluor 594 (1:500, Jackson ImmunoResearch), and rat anti-mouse Alexa Fluor 594
712 (1:200, Abcam). Sections were mounted with DAPI-containing mounting medium (ProTaqs
713 MountFluor Anti-Fading).
714 Images were captured using a Zeiss Axioscan.Z1 slide scanner, and morphometric and
715 fluorescence analyses were performed with ImageJ software.

716 In H&E and MT-stained images, blood vessels were identified by luminal structures containing
717 erythrocytes. Vessel numbers within grafts were quantified, and vessel/graft and vessel/β-cell
718 ratios were calculated as percentages of graft and insulin-positive areas. Human vasculature was
719 confirmed by erythrocyte-containing vessels positive for human CD31 and α-SMA staining.
720

721 **Statistical analysis**

722 Statistical analyses were performed using GraphPad Prism 10.0. All experiments were repeated at
723 least three times. Specific statistical tests are detailed in the figure legends, with significance
724 defined as $P < 0.05$.

725 **List of Supplementary Materials**

726 Materials and Methods
727 Fig. S1 or Fig S9
728 Table S1
729 References (*1,2*)
730
731
732
733
734
735
736
737
738
739
740

741 **References and Notes**

742

743 1. L. A. DiMeglio, C. Evans-Molina, R. A. Oram, Type 1 diabetes. *Lancet* **391**, 2449-2462 (2018).
744 2. F. B. Barton *et al.*, Improvement in outcomes of clinical islet transplantation: 1999-2010.
745 *Diabetes care* **35**, 1436-1445 (2012).
746 3. A. M. Shapiro, M. Pokrywczynska, C. Ricordi, Clinical pancreatic islet transplantation. *Nature*
747 *reviews. Endocrinology* **13**, 268-277 (2017).
748 4. B. W. Paty, J. S. Harmon, C. L. Marsh, R. P. Robertson, Inhibitory effects of immunosuppressive
749 drugs on insulin secretion from HIT-T15 cells and Wistar rat islets. *Transplantation* **73**, 353-357
750 (2002).
751 5. L. Reid, F. Baxter, S. Forbes, Effects of islet transplantation on microvascular and macrovascular
752 complications in type 1 diabetes. *Diabetic medicine : a journal of the British Diabetic Association*
753 **38**, e14570 (2021).
754 6. E. A. Ryan, B. W. Paty, P. A. Senior, A. M. Shapiro, Risks and side effects of islet transplantation.
755 *Curr Diab Rep* **4**, 304-309 (2004).
756 7. M. Biarnés, M. Montolio, V. Nacher, M. Raurell, J. Soler, E. Montanya, Beta-cell death and mass
757 in syngeneically transplanted islets exposed to short- and long-term hyperglycemia. *Diabetes* **51**,
758 66-72 (2002).
759 8. G. L. Jones, M. T. Juszczak, S. J. Hughes, P. Kooner, S. H. Powis, M. Press, Time course and
760 quantification of pancreatic islet revascularization following intraportal transplantation. *Cell*
761 *transplantation* **16**, 505-516 (2007).
762 9. W. Moritz *et al.*, Apoptosis in hypoxic human pancreatic islets correlates with HIF-1alpha
763 expression. *Faseb j* **16**, 745-747 (2002).
764 10. J. Tjernberg, K. N. Ekdahl, J. D. Lambris, O. Korsgren, B. Nilsson, Acute antibody-mediated
765 complement activation mediates lysis of pancreatic islets cells and may cause tissue loss in
766 clinical islet transplantation. *Transplantation* **85**, 1193-1199 (2008).
767 11. D. M. Berman *et al.*, Bioengineering the Endocrine Pancreas: Intraomental Islet Transplantation
768 Within a Biologic Resorbable Scaffold. *Diabetes* **65**, 1350-1361 (2016).
769 12. E. Cantarelli *et al.*, Bone marrow as an alternative site for islet transplantation. *Blood* **114**, 4566-
770 4574 (2009).
771 13. Z. Kakabadze, S. Gupta, D. Brandhorst, O. Korsgren, E. Berishvili, Long-term engraftment and
772 function of transplanted pancreatic islets in vascularized segments of small intestine. *Transpl Int*
773 **24**, 175-183 (2011).
774 14. Z. Kakabadze *et al.*, Correction of diabetes mellitus by transplanting minimal mass of syngeneic
775 islets into vascularized small intestinal segment. *Am J Transplant* **13**, 2550-2557 (2013).
776 15. Z. Kakabadze, K. Shanava, C. Ricordi, A. M. Shapiro, S. Gupta, E. Berishvili, An isolated venous sac
777 as a novel site for cell therapy in diabetes mellitus. *Transplantation* **94**, 319-324 (2012).
778 16. F. Pattou, J. Kerr-Conte, D. Wild, GLP-1-receptor scanning for imaging of human beta cells
779 transplanted in muscle. *The New England journal of medicine* **363**, 1289-1290 (2010).
780 17. E. Rafael *et al.*, Intramuscular autotransplantation of pancreatic islets in a 7-year-old child: a 2-
781 year follow-up. *Am J Transplant* **8**, 458-462 (2008).
782 18. A. Sterkers *et al.*, Islet survival and function following intramuscular autotransplantation in the
783 minipig. *Am J Transplant* **13**, 891-898 (2013).
784 19. M. Yu *et al.*, Islet transplantation in the subcutaneous space achieves long-term euglycaemia in
785 preclinical models of type 1 diabetes. *Nature metabolism* **2**, 1013-1020 (2020).

786 20. M. J. Quizon, A. J. García, Engineering β Cell Replacement Therapies for Type 1 Diabetes:
787 Biomaterial Advances and Considerations for Macroscale Constructs. *Annual review of*
788 *pathology* **17**, 485-513 (2022).
789 21. R. Hanna, E. Berishvili, Advances and challenges of endocrine pancreas bioengineering. *Current*
790 *Opinion in Endocrine and Metabolic Research* **23**, 100320 (2022).
791 22. T. Berney *et al.*, From islet of Langerhans transplantation to the bioartificial pancreas. *Presse*
792 *medicale (Paris, France : 1983)*, 104139 (2022).
793 23. A. D. Agulnick *et al.*, Insulin-Producing Endocrine Cells Differentiated In Vitro From Human
794 Embryonic Stem Cells Function in Macroencapsulation Devices In Vivo. *Stem cells translational*
795 *medicine* **4**, 1214-1222 (2015).
796 24. P. O. Carlsson *et al.*, Transplantation of macroencapsulated human islets within the bioartificial
797 pancreas βAir to patients with type 1 diabetes mellitus. *Am J Transplant* **18**, 1735-1744 (2018).
798 25. A. M. J. Shapiro *et al.*, Insulin expression and C-peptide in type 1 diabetes subjects implanted
799 with stem cell-derived pancreatic endoderm cells in an encapsulation device. *Cell reports.*
800 *Medicine* **2**, 100466 (2021).
801 26. M. Barillaro, M. Schuurman, R. Wang, β1-Integrin—A Key Player in Controlling Pancreatic Beta-
802 Cell Insulin Secretion via Interplay With SNARE Proteins. *Endocrinology* **164**, (2022).
803 27. L. Rosenberg, R. Wang, S. Paraskevas, D. Maysinger, Structural and functional changes resulting
804 from islet isolation lead to islet cell death. *Surgery* **126**, 393-398 (1999).
805 28. M. Riopel, R. Wang, Collagen matrix support of pancreatic islet survival and function. *Frontiers in*
806 *bioscience (Landmark edition)* **19**, 77-90 (2014).
807 29. S. Saleem, J. Li, S. P. Yee, G. F. Fellows, C. G. Goodyer, R. Wang, beta1 integrin/FAK/ERK
808 signalling pathway is essential for human fetal islet cell differentiation and survival. *The Journal*
809 *of pathology* **219**, 182-192 (2009).
810 30. C. H. Stephens *et al.*, Oligomeric collagen as an encapsulation material for islet/β-cell
811 replacement: effect of islet source, dose, implant site, and administration format. *Am J Physiol*
812 *Endocrinol Metab* **319**, E388-e400 (2020).
813 31. A. E. Vlahos, N. Cober, M. V. Sefton, Modular tissue engineering for the vascularization of
814 subcutaneously transplanted pancreatic islets. *Proceedings of the National Academy of Sciences*
815 *of the United States of America* **114**, 9337-9342 (2017).
816 32. D. M. Tremmel *et al.*, A human pancreatic ECM hydrogel optimized for 3-D modeling of the islet
817 microenvironment. *Scientific Reports* **12**, 7188 (2022).
818 33. D. A. Baidal *et al.*, Bioengineering of an Intraabdominal Endocrine Pancreas. *The New England*
819 *journal of medicine* **376**, 1887-1889 (2017).
820 34. F. Lebreton *et al.*, Insulin-producing organoids engineered from islet and amniotic epithelial cells
821 to treat diabetes. *Nature communications* **10**, 4491 (2019).
822 35. P. M. Crapo, T. W. Gilbert, S. F. Badylak, An overview of tissue and whole organ decellularization
823 processes. *Biomaterials* **32**, 3233-3243 (2011).
824 36. A. Citro *et al.*, Biofabrication of a vascularized islet organ for type 1 diabetes. *Biomaterials* **199**,
825 40-51 (2019).
826 37. W. R. Loewenstein, Junctional intercellular communication: the cell-to-cell membrane channel.
827 *Physiol Rev* **61**, 829-913 (1981).
828 38. J. Chen, J. E. Gunton, Beta-cell function and human islet transplantation: can we improve? *J*
829 *Endocrinol* **248**, R99-r112 (2021).
830 39. P. Dunér *et al.*, Adhesion G Protein-Coupled Receptor G1 (ADGRG1/GPR56) and Pancreatic β-
831 Cell Function. *J Clin Endocrinol Metab* **101**, 4637-4645 (2016).

832 40. O. Cabrera, D. M. Berman, N. S. Kenyon, C. Ricordi, P. O. Berggren, A. Caicedo, The unique
833 cytoarchitecture of human pancreatic islets has implications for islet cell function. *Proceedings*
834 *of the National Academy of Sciences of the United States of America* **103**, 2334-2339 (2006).
835 41. P. Rorsman, F. M. Ashcroft, Pancreatic β-Cell Electrical Activity and Insulin Secretion: Of Mice
836 and Men. *Physiol Rev* **98**, 117-214 (2018).
837 42. M. Brissova *et al.*, Human Islets Have Fewer Blood Vessels than Mouse Islets and the Density of
838 Islet Vascular Structures Is Increased in Type 2 Diabetes. *J Histochem Cytochem* **63**, 637-645
839 (2015).
840 43. C. Dai *et al.*, Islet-enriched gene expression and glucose-induced insulin secretion in human and
841 mouse islets. *Diabetologia* **55**, 707-718 (2012).
842 44. A. R. Pepper, C. Gall, D. M. Mazzuca, C. W. Melling, D. J. White, Diabetic rats and mice are
843 resistant to porcine and human insulin: flawed experimental models for testing islet xenografts.
844 *Xenotransplantation* **16**, 502-510 (2009).
845 45. M. Wunderlich *et al.*, A xenograft model of macrophage activation syndrome amenable to anti-
846 CD33 and anti-IL-6R treatment. *JCI Insight* **1**, e88181 (2016).
847 46. M. Hu, W. J. Hawthorne, S. Yi, P. J. O'Connell, Cellular Immune Responses in Islet Xenograft
848 Rejection. *Front Immunol* **13**, 893985 (2022).
849 47. M. Vadori, E. Cozzi, Immunological challenges and therapies in xenotransplantation. *Cold Spring*
850 *Harb Perspect Med* **4**, a015578 (2014).
851 48. A. Lam *et al.*, Estimation of Early Graft Function Using the BETA-2 Score Following Clinical Islet
852 Transplantation. *Transpl Int* **35**, 10335 (2022).
853 49. M. Chetboun *et al.*, Association between primary graft function and 5-year outcomes of islet
854 allogeneic transplantation in type 1 diabetes: a retrospective, multicentre, observational cohort
855 study in 1210 patients from the Collaborative Islet Transplant Registry. *Lancet Diabetes*
856 *Endocrinol* **11**, 391-401 (2023).
857 50. S. E. Townsend, M. Gannon, Extracellular Matrix–Associated Factors Play Critical Roles in
858 Regulating Pancreatic β-Cell Proliferation and Survival. *Endocrinology* **160**, 1885-1894 (2019).
859 51. C. Pignatelli, F. Campo, A. Neroni, L. Piemonti, A. Citro, Bioengineering the Vascularized
860 Endocrine Pancreas: A Fine-Tuned Interplay Between Vascularization, Extracellular-Matrix-Based
861 Scaffold Architecture, and Insulin-Producing Cells. *Transpl Int* **35**, 10555 (2022).
862 52. A. Citro *et al.*, Directed self-assembly of a xenogeneic vascularized endocrine pancreas for type 1
863 diabetes. *Nature communications* **14**, 878 (2023).
864 53. J. D. Weaver *et al.*, Vasculogenic hydrogel enhances islet survival, engraftment, and function in
865 leading extrahepatic sites. *Sci Adv* **3**, e1700184 (2017).
866 54. E. A. Phelps, K. L. Templeman, P. M. Thulé, A. J. García, Engineered VEGF-releasing PEG-MAL
867 hydrogel for pancreatic islet vascularization. *Drug Deliv Transl Res* **5**, 125-136 (2015).
868 55. D. M. Tremmel *et al.*, A human pancreatic ECM hydrogel optimized for 3-D modeling of the islet
869 microenvironment. *Sci Rep* **12**, 7188 (2022).
870 56. X. Hu, Z. Wu, Z. Zhang, H. Yao, D.-A. Wang, Type II collagen scaffolds for tissue engineering.
871 *Communications Materials* **5**, 149 (2024).
872 57. S. Ullah, I. Zainol, Fabrication and applications of biofunctional collagen biomaterials in tissue
873 engineering. *Int J Biol Macromol* **298**, 139952 (2025).
874 58. M. Abedi, M. Shafiee, F. Afshari, H. Mohammadi, Y. Ghasemi, Collagen-Based Medical Devices
875 for Regenerative Medicine and Tissue Engineering. *Appl Biochem Biotechnol* **196**, 5563-5603
876 (2024).
877 59. R. Tamburrini *et al.*, Detergent-Free Decellularization of the Human Pancreas for Soluble
878 Extracellular Matrix (ECM) Production. *J Vis Exp*, (2020).

879 60. L. Somasekhar, L. G. Griffiths, Current Challenges and Future Promise for Use of Extracellular
880 Matrix Scaffold to Achieve the Whole Organ Tissue Engineering Moonshot. *Stem cells*
881 *translational medicine* **12**, 588-602 (2023).
882 61. J. Fernández-Pérez, M. Ahearne, The impact of decellularization methods on extracellular matrix
883 derived hydrogels. *Scientific Reports* **9**, 14933 (2019).
884 62. M. Kasravi *et al.*, Immunogenicity of decellularized extracellular matrix scaffolds: a bottleneck in
885 tissue engineering and regenerative medicine. *Biomater Res* **27**, 10 (2023).
886 63. A. Asthana *et al.*, Comprehensive characterization of the human pancreatic proteome for
887 bioengineering applications. *Biomaterials* **270**, 120613 (2021).
888 64. Z. Li *et al.*, Proteome-wide and matrisome-specific alterations during human pancreas
889 development and maturation. *Nature communications* **12**, 1020 (2021).
890 65. Z. Hu *et al.*, Biological importance of human amniotic membrane in tissue engineering and
891 regenerative medicine. *Mater Today Bio* **22**, 100790 (2023).
892 66. F. Dadkhah Tehrani, A. Firouzeh, I. Shabani, A. Shabani, A Review on Modifications of Amniotic
893 Membrane for Biomedical Applications. *Frontiers in bioengineering and biotechnology* **8**, 606982
894 (2020).
895 67. M. Doucette *et al.*, Early Advanced Therapy for Diabetic Foot Ulcers in High Amputation Risk
896 Veterans: A Cohort Study. *Int J Low Extrem Wounds* **21**, 111-119 (2022).
897 68. I. Schmiedova, Z. Ozanova, E. Stastna, L. Kiselakova, B. Lipovy, S. Forostyak, Case Report: Freeze-
898 Dried Human Amniotic Membrane Allograft for the Treatment of Chronic Wounds: Results of a
899 Multicentre Observational Study. *Frontiers in bioengineering and biotechnology* **9**, 649446
900 (2021).
901 69. B. Lipový, M. Hladík, P. Štourač, S. Forostyak, Case Report: Wound Closure Acceleration in a
902 Patient With Toxic Epidermal Necrolysis Using a Lyophilised Amniotic Membrane. *Frontiers in*
903 *bioengineering and biotechnology* **9**, 649317 (2021).
904 70. E. Berishvili *et al.*, ESOT Roadmap for Advanced Therapy Medicinal Products in Transplantation:
905 Navigating Regulatory Challenges to Enhance Access and Care. *Transpl Int* **37**, 13485 (2024).
906 71. S. E. Cross *et al.*, Key Matrix Proteins Within the Pancreatic Islet Basement Membrane Are
907 Differentially Digested During Human Islet Isolation. *Am J Transplant* **17**, 451-461 (2017).
908 72. L. A. Llacua, M. M. Faas, P. de Vos, Extracellular matrix molecules and their potential
909 contribution to the function of transplanted pancreatic islets. *Diabetologia* **61**, 1261-1272
910 (2018).
911 73. M. M. Riopel, J. Li, S. Liu, A. Leask, R. Wang, β1 integrin–extracellular matrix interactions are
912 essential for maintaining exocrine pancreas architecture and function. *Laboratory Investigation*
913 **93**, 31-40 (2013).
914 74. J. Peart, J. Li, H. Lee, M. Riopel, Z. C. Feng, R. Wang, Critical role of β1 integrin in postnatal beta-
915 cell function and expansion. *Oncotarget* **8**, 62939-62952 (2017).
916 75. C. P. Carvalho *et al.*, Beta cell coupling and connexin expression change during the functional
917 maturation of rat pancreatic islets. *Diabetologia* **53**, 1428-1437 (2010).
918 76. P. Klee *et al.*, Connexin implication in the control of the murine beta-cell mass. *Pediatr Res* **70**,
919 142-147 (2011).
920 77. N. L. Farnsworth, R. K. Benninger, New insights into the role of connexins in pancreatic islet
921 function and diabetes. *FEBS Lett* **588**, 1278-1287 (2014).
922 78. Y. Guo, C. Martinez-Williams, C. E. Yellowley, H. J. Donahue, D. E. Rannels, Connexin expression
923 by alveolar epithelial cells is regulated by extracellular matrix. *Am J Physiol Lung Cell Mol Physiol*
924 **280**, L191-202 (2001).
925 79. S. Imbeault *et al.*, The extracellular matrix controls gap junction protein expression and function
926 in postnatal hippocampal neural progenitor cells. *BMC Neurosci* **10**, 13 (2009).

80. H. Peiris, C. S. Bonder, P. T. Coates, D. J. Keating, C. F. Jessup, The β-cell/EC axis: how do islet cells talk to each other? *Diabetes* **63**, 3-11 (2014).
81. G. Burganova, C. Bridges, P. Thorn, L. Landsman, The Role of Vascular Cells in Pancreatic Beta-Cell Function. *Frontiers in endocrinology* **12**, 667170 (2021).
82. G. Parnaud, E. Hammar, D. G. Rouiller, M. Armanet, P. A. Halban, D. Bosco, Blockade of beta1 integrin-laminin-5 interaction affects spreading and insulin secretion of rat beta-cells attached on extracellular matrix. *Diabetes* **55**, 1413-1420 (2006).
83. L. M. Fonseca, N. Krause, F. Lebreton, E. Berishvili, Recreating the Endocrine Niche: Advances in Bioengineering the Pancreas. *Artif Organs*, (2025).
84. J. Sellarés *et al.*, Understanding the causes of kidney transplant failure: the dominant role of antibody-mediated rejection and nonadherence. *Am J Transplant* **12**, 388-399 (2012).
85. E. Pouliquen *et al.*, Recent advances in renal transplantation: antibody-mediated rejection takes center stage. *F1000Prime Rep* **7**, 51 (2015).
86. C. C. Chen *et al.*, Endothelial chimerism and vascular sequestration protect pancreatic islet grafts from antibody-mediated rejection. *J Clin Invest* **128**, 219-232 (2018).
87. M. Naesens *et al.*, The Banff 2022 Kidney Meeting Report: Reappraisal of microvascular inflammation and the role of biopsy-based transcript diagnostics. *Am J Transplant* **24**, 338-349 (2024).
88. X. Charmetant, G. J. Pettigrew, O. Thaunat, Allorecognition Unveiled: Integrating Recent Breakthroughs Into the Current Paradigm. *Transpl Int* **37**, 13523 (2024).
89. A. Koenig *et al.*, Missing self triggers NK cell-mediated chronic vascular rejection of solid organ transplants. *Nature communications* **10**, 5350 (2019).
90. O. Thaunat, Natural killer cell-mediated innate microvascular rejection. *Nat Rev Nephrol* **20**, 489-490 (2024).
91. V. Coppens *et al.*, Human blood outgrowth endothelial cells improve islet survival and function when co-transplanted in a mouse model of diabetes. *Diabetologia* **56**, 382-390 (2013).
92. T. Mathur *et al.*, Organ-on-chips made of blood: endothelial progenitor cells from blood reconstitute vascular thromboinflammation in vessel-chips. *Lab Chip* **19**, 2500-2511 (2019).
93. C. Olgasi *et al.*, Efficient and safe correction of hemophilia A by lentiviral vector-transduced BOECs in an implantable device. *Mol Ther Methods Clin Dev* **23**, 551-566 (2021).
94. H. Peiris, C. S. Bonder, P. T. H. Coates, D. J. Keating, C. F. Jessup, The β-Cell/EC Axis: How Do Islet Cells Talk to Each Other? *Diabetes* **63**, 3-11 (2013).
95. R. L. Thom, A. J. Cronin, Legal and Regulatory Challenges for Emerging Regenerative Medicine Solutions for Diabetes. *Transplantation* **108**, 1072-1079 (2024).

Funding: This work is supported by grants from the European Commission (Horizon 2020 Framework Program; VANGUARD grant 874700), the Breakthrough T1D, formerly JDRF (JDRF; grant 3-SRA-2020-926-S-B and 3-SRA-2023-1441-S-B) and the Swiss National Science Foundation (grant 310030_213013 and CRSII5_209417).

968 **Author contributions:** E.B. conceptualized and supervised the project.; E.B. and K.B. developed
969 the methodology; K.B., F.L. and M.H. performed animal breeding and conducted experiments;
970 K.B., F.L., M.H., R.H., J.B., A.M., L.M.F., and F.C. performed analysis of results; K.B., and M.H.
971 performed visualization.; A.F. and A.C. produced BOECs; E.B. K.B. and F.L. wrote the original
972 draft.; A.F., L.P., O.T., J.S, M.C. and E.B. contributed to the design of the experiments.; A.F.,
973 C.O., J.B., A.M., L.M.F., M.C., B.MT., L.P., A.C., O.T., J.S., M.H., L.WB., P.C. and
974 VANGUARD consortium critically reviewed and edited the paper.

975 **Competing interests:** Authors declare that they have no competing interests.

976 **Data and materials availability:** All data are available in the main text or the supplementary
977 materials.

978

979

980 **§ Members of the VANGUARD consortium are as follows:**

981 Thierry Berney, Nicerine Krause, Shota Tsikhiseli, University of Geneva, Department of
982 Surgery, Geneva, Switzerland
983 Alessia Cucci, Chiara Borsotti, Simone Assanelli, Department of Health Sciences, University of
984 Piemonte Orientale, Novara, Italy
985 Cataldo Pignatelli, IRCCS Ospedale San Raffaele, Diabetes Research Institute, Milano, Italy
986 Emma Massey, Dide de Jongh, Erasmus MC, University Medical Centre Rotterdam, The
987 Netherlands
988 Eline Bunnik, Dept. of Medical Ethics, Philosophy and History of Medicine, University Medical
989 Centre Rotterdam, The Netherlands
990 Antonia J. Cronin, King's College, London, UK
991 Devi Mey, Chiara Parisotto European Society for Organ Transplantation, Padova, Italy

Patrick Kugelmeier, Petra Wolint, Kugelmeiers AG, Erlenbach, Switzerland

Margaryta Schaltegger, Julia Götz, Jeanette Müller, Accelopment Switzerland Ltd.